Analytica Chimica Acta 1330 (2024) 343269

Contents lists available at ScienceDirect

Analytica Chimica Acta

journal homepage: www.elsevier.com/locate/aca

Optimization of nanoparticle-enhanced laser-induced breakdown spectroscopy for the hyperspectral chemical mapping of solid samples

Fernando A. Casian-Plaza [a], Dávid J. Palásti [a], Félix Schubert [b], Gábor Galbács [a,*]

[a] Department of Molecular and Analytical Chemistry, University of Szeged, Dóm Square 7-8., 6720, Szeged, Hungary
[b] Department of Mineralogy, Geochemistry and Petrology, University of Szeged, Egyetem Street 2., 6722, Szeged, Hungary

HIGHLIGHTS

- Analytical capabilities of nanoparticle-enhanced LIBS mapping are studied in detail.
- Impact of the experimental conditions on the signal enhancement is investigated.
- Analytical applications (one quantitative and one qualitative) are demonstrated.
- Significant improvement is provided by NE-LIBS mapping in spatial discrimination studies.

GRAPHICAL ABSTRACT

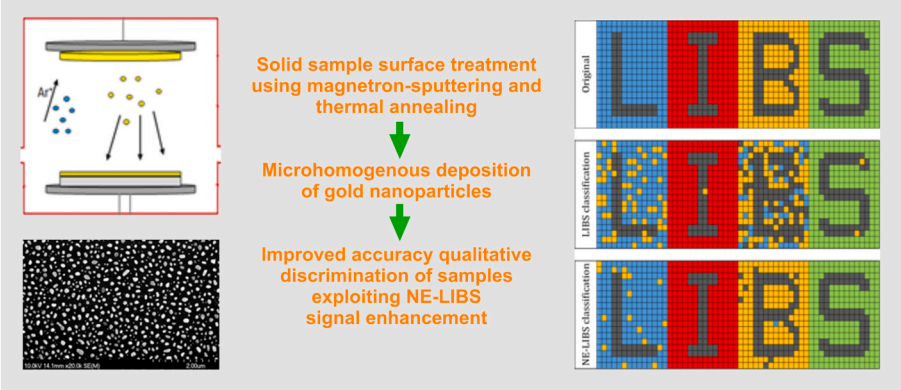

ARTICLE INFO

Keywords:
Magnetron sputtering
Nanoparticle-enhanced laser-induced breakdown spectroscopy (NE-LIBS)
Spatial classification
Qualitative discrimination

ABSTRACT

Background: Nanoparticle-enhanced laser-induced breakdown spectroscopy (NE-LIBS) uses the plasmonic effect of metallic nanoparticles deposited on solid sample surfaces to achieve a significant signal enhancement by lowering the breakdown threshold and elevating plasma temperature. NE-LIBS has been used for localized analysis, but NE-LIBS mapping of solids has rarely been done, due to several challenges. In this study, we scrutinized the performance of NE-LIBS hyperspectral mapping of solid samples, when the controlled deposition of nanoparticles was done using magnetron sputtering.

Results: We performed a detailed optimization of the nanoparticle-related signal enhancement involving the laser wavelength, laser fluence and detector gating. It was confirmed that while the laser wavelength has only a small influence in the studied range (at 266 nm, 532 nm and 1064 nm), but there is an optimum for laser fluence and detection gate delay. The best signal enhancement achieved for a glass sample was 25–30. The applicability of the approach was demonstrated by hyperspectral NE-LIBS mapping of a granite rock sample, which provided an improved sensitivity in the study of the elemental distribution (exemplified for Li and Mg), and by paint linear discriminant analysis, in which NE-LIBS gave rise to a significantly improved accuracy (98 %, as opposed to the LIBS accuracy of only 84 %).

* Corresponding author.
E-mail address: galbx@chem.u-szeged.hu (G. Galbács).

https://doi.org/10.1016/j.aca.2024.343269
Received 6 June 2024; Received in revised form 17 September 2024; Accepted 19 September 2024
Available online 20 September 2024

Significance: The analytical benefits of NE-LIBS hyperspectral mapping was demonstrated in two applications involving industrially relevant sample types. For example, the enhanced signals in rock elemental mapping can improve the localization of mineral grains viable for economic mining. The qualitative discrimination application involving paints demonstrates that the NE-LIBS approach can be beneficial in the spatial classification or identification of the local quality of a solid sample surface.

1. Introduction

Laser-induced breakdown spectroscopy (LIBS) offers many analytical benefits for the sensitive investigation of solid samples and hence it is becoming increasingly popular both in science and the industry. High sample throughput, ppm-level trace analytical limits of detection, practically no sample preparation, possibility for in-field or stand-off operation are only a few of the advantageous characteristics of LIBS spectroscopy [1–4]. LIBS spectra contain a large amount of chemical information, which can not only be used for quantitative multielemental analysis, but they can also serve as a "spectral fingerprint" based on which local sample quality can be identified or classified.

An application area in which LIBS proved itself very useful in recent years is elemental mapping [5–11]. One of the strengths of LIBS's popularity in this field is that it combines a true hyperspectral approach with single-shot trace analytical sensitivity [7,12]. The provided some tens of μm range spatial resolution can be utilized in a wide range of applications and what is also important, for all elements, light or heavy. Taking advantage of the ablative character of LIBS, layer-by-layer depth-resolved mapping is also possible for depths of up to a few hundred micrometers [5].

Signal enhancement is a prominent research direction in the LIBS field, and several techniques (e.g. the use of double or multiple laser pulses, plasma confinement or plasma reheating using external sources of energy, etc.) have been proposed and tested already [1,13,14]. The nanoparticle-enhanced LIBS (NE-LIBS) is one of the more practical approaches, which can offer a factor of ca. 3–100 signal enhancement, and it only requires the deposition of plasmonic (e.g. gold) nanoparticles (NPs) on the solid sample surface prior to LIBS analysis [15,16]. Detailed studies, mostly published by the De Giacomo group, shedded light on the mechanisms behind the signal enhancement as well as the influence of several experimental conditions [17–19]. It was shown that the effect is related to the coupling of surface plasmons excited in the metallic NPs, which increases the electrical field strength, promoting the release of seed electrons for plasma formation. In the past few years, the NE-LIBS field is flourishing and many studies have appeared in the literature that exploited the nanoparticle enhancement. This is also demonstrated by, for example, that the approach has been applied to not only solid, but also liquid [20,21] and most recently even gaseous [22] sample analysis. The successfully analyzed sample types also range widely from cement [23] over human serum [21] to proteins [24,25], just to name a few. Most NE-LIBS works use gold NPs, but the application of other plasmonic NPs, such as silver [20,21] and copper [26] also occur.

Clearly, LIBS elemental or chemical mapping could also benefit from the signal enhancement related to the application of nanoparticles. A couple of research groups have already reported about the successful use of the NE-LIBS approach for mapping on metallic [27], plant [28] and glass samples [29]. However, it became also clear that there are some challenges that need to be tackled for the successful application of NE-LIBS to mapping. Namely, *a.*) a proper, controllable NP deposition technique must be used to ensure the homogeneous deposition and hence comparable and reliable signal enhancement across the sample surface, *b.*) deposited NPs should not excessively relocate upon the action of the shockwave generated by the sequence of laser ablations in the vicinity of the analytical spots, *c.*) the laser spot size can not be too small in order to allow for the efficient coupling of the surface plasmons. In one of our recent studies [29], we investigated these challenges in detail and demonstrated that magnetron sputtering followed by thermal treatment can produce NP deposition with suitable control options and laser ablation characteristics for NE-LIBS mapping. We also showed that ca. 200 μm spot size can be a good compromise between signal enhancement and spatial resolution.

In the present work, we studied the effect of wavelength, detector gating and laser fluence in an effort to optimize the NE-LIBS signal enhancement for mapping applications using the sputtering-based sample preparation protocol we developed [29]. We also provide demonstrations for two analytical applications of the proposed NE-LIBS hyperspectral mapping methodology: elemental mapping of a granite rock for the localization of mineral grains containing elevated concentrations of technologically relevant elements such as Li, and the spatial classification of black paints.

2. Materials and methods

2.1. Nanoparticle deposition

Magnetron sputtering deposition was performed using a Quorum Q150RS Plus (Quorum Technologies, UK) rotary-pumped coater, on soda-lime glass microscope slides as substrates (Epredia, Germany). Sputtering was accomplished from a high purity, 57 mm diameter, 0.1 mm thick gold target (99.99 %, Goodfellow Cambridge Ltd., UK). The target-substrate distance was 60 mm. We kept the current at 20 mA and the argon pressure at 0.1 mbar, while the substrate was rotated with a speed of 25 rpm. Sputtering time was fixed at 240 s. The deposited gold thin film was subjected to thermal treatment in a muffle furnace (Thermolyne 62700, USA) at 550 °C for 20 min and the samples were left to cool down at room temperature. This combination of sputtering and thermal treatment was found to provide a homogeneous deposition of gold NPs with suitable size distribution and interparticle distances for NE-LIBS [29].

2.2. LIBS measurements

All LIBS measurements at 266 nm laser wavelengths were performed using a J200 LIBS/LA tandem instrument (Applied Spectra, USA) equipped with a Q-switched Nd:YAG laser source operating at 266 nm with a pulse duration of 6 ns. The LIBS detection system consisted of a six-channel CCD spectrometer with a spectral coverage of 190–1040 nm and a resolution of 0.07 nm. The system was controlled by Applied Spectra's Axiom LA 2.4 operation software, typically employing a 0.5 μs gate delay and 1 ms gate width. Experiments were carried out under constant argon flow with a rate of 1 L min^{-1}. NE-LIBS scanning/mapping measurements were carried out employing stepwise scans with non-overlapping 200 μm spot sizes. If not indicated otherwise, the pulse energy applied was 18 mJ, which corresponded to a fluence of 56 J cm^{-2}.

LIBS experiments performed with 532 nm and 1064 nm laser wavelengths were carried out using a Quantel Ultra 100 laser source equipped with a frequency upconversion unit (this laser source is actually identical to the one incorporated in our the ASI J-200 LA/LIBS instrument, except for the harmonic unit). Laser light was focused on the sample surface by using a plano-convex quartz lens (f = 50 mm) and the plasma emission was collected at a 45° angle via a NA-matched quartz focusing lens into an optical fiber.

In LIBS experiments at 532 nm or 1064 nm, or which needed a high time resolution, were performed using an Echelle spectrometer (Aryelle

200, LTB, Germany) equipped with a gated ICCD camera detector (iStar DH334T-18F-04, Andor Technology, Ireland). Plasma emission within the J200 LIBS instrument was collected via a fiber optic-based alternative light collection sub-system custom-made for our laboratory by ASI Inc. It uses an optical fiber with a 400 μm core diameter and delivers the light to the 40 μm entrance slit of our Echelle spectrometer. Emission spectra in this configuration were recorded in the spectral range of 220–629 nm, with a resolving power exceeding 9000. The detector gate width was set at 1000 ns while the gate delay was varied from 0 to 5 μs, using the built-in digital delay generator of the camera. Fig. 1 gives an overview of the experimental setup.

2.3. Samples and their preparation for LIBS and NE-LIBS elemental mapping

In the experiments involving a rock sample, a monzogranite type granitoid rock from Hungary, was used. The rock was cut using a diamond cutter (DiscoPlan, Struers, Denmark) to expose a 20 × 20 mm area. The surface was fine-polished using a LaboPOL-35 machine (Struers, Denmark) using 500- and 1200-grit MD-Piano (Struers, Denmark) diamond grinding wheels. As a final step, the aqueous suspension of SiC abrasive powder (Buehler, USA) was applied to smoothen the sample surface and then the sample was carefully rinsed with trace quality deionized water and analytical purity ethanol, applying lint-free cleaning wipes (Kimwipes, USA). For a microscope image of the studied surface of the rock sample, please see section 3.2.1.

For the experiments regarding paint discrimination analysis, five different, heat resistant (600–800 °C), commercial black paints, meant for automotive use, were obtained from different manufacturers. The paints were applied to a stainless-steel plate substrates from a distance of ca. 30 cm. Photographs of the painted plates can be seen in Fig. 2. As it can be seen, only very slight hue and reflectivity variations may be observed between the paints by the naked eye. Paint differentiation therefore requires instrumental measurements, like the chemometric evaluation of their LIBS spectra, as described in section 3.2.2. Three layers of paint were applied, with a wait of 15 min for drying between the layers. The painting process was followed by a 1 h, 160 °C baking in an oven (UNE 400, Memmert, Germany), in accordance with the manufacturer's instructions. The number of layers necessary to avoid the ablation of the steel substrate during the LIBS experiments was established by performing depth-resolved measurements with the laser settings used later in the mapping experiments and monitoring the spectra (we made test samples with a different number of paint layers on the steel pieces and then we painted a thicknesses that ensured that the laser pulse did not penetrate the paint, so there was no contribution to the paint spectrum from the steel).

2.4. Data evaluation

LIBS data processing and elemental map generation was primarily carried out in the ClarityNeXt 1.0 software (Applied Spectra, USA). SEM images were analyzed by the open source, Java-based ImageJ software in order to calculate the mean particle diameter and interparticle distances. All graphs were prepared in Origin 9.0 (OriginLabs, USA).

Two well-established chemometric methods, namely linear discriminant analysis (LDA) and principal component analysis (PCA) were used to process the LIBS data for qualitative discrimination purposes. PCA is one of the most commonly used data compression methods. It projects the measurements into a new space, where none of the variables are correlated, and aims to describe the data as best as possible. It is often used for the visualization of high-dimensionality data and data pre-processing for other chemometric methods. LDA is considered a data projection method, but the projection is not used to describe the dataset, but to highlight the differences between existing groups. Details of these methods are described in most chemometric textbooks, such as in Ref. [30]. PCA and LDA data processing and visualization was done using the open-source R Studio Desktop software package (v1.3), developing custom codes using the Chemometrics and MASS packages.

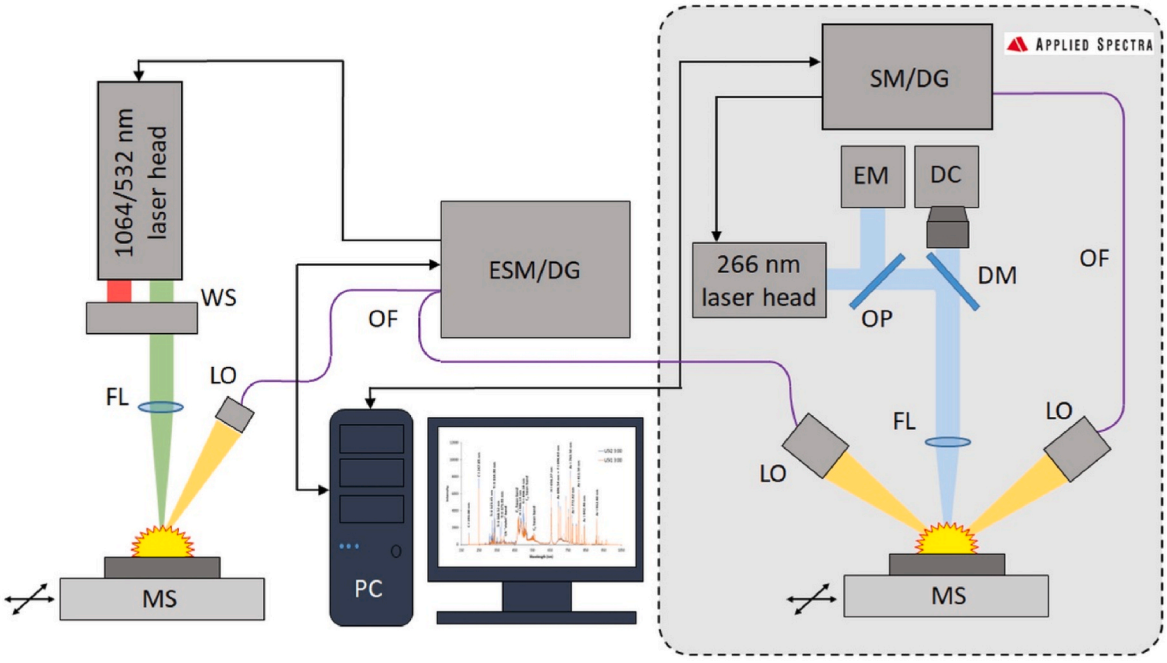

Fig. 1. An overview of the experimental setup. Equipment on the right encircled with a dashed line indicates the relevant components inside the J-200 LIBS instrument. SM/DG – Spectrometer with delay generator, ESM/DG – Echelle spectrometer with delay generator, WS - Wavelength selector, OP - Outcoupling plate, EM - Energy meter, DM - Dichroic mirror, DC - Digital camera, MS - Motorized sample stage, LO - Light collection optics, OF – Optical fiber, FL – Focusing lens.

Fig. 2. Photographs of the five stainless steel samples coated with different black paints.

3. Results and discussion

3.1. Signal enhancement

As it was alluded to before, it is known from the NE-LIBS literature that the signal enhancement (SE, the ratio of the signals obtained with and without NPs) achievable depends strongly on the experimental parameters related to the laser, nanoparticles and sample (substrate). The effects of these are also interrelated. Here we assessed the influence of some of them on the SE with respect to the presently applied sputtering NP deposition technique and for a soda-lime glass sample.

3.1.1. Effect of laser fluence

The laser fluence has a complex effect on the achievable signal enhancement. De Giacomo and co-workers observed that the SE *vs* laser fluence plot follows a maximum curve, which they attributed to non-linear effects responsible for the excitation of electrons resulting in the generation of hot electrons and effective charge separation [18]. As it can be seen from Fig. 3., our experiments also confirmed that there is an optimum value for the fluence, due to the fact that although both NE-LIBS and LIBS signals increase with an increasing fluence, but in a certain range, the former outgrows the latter. For our experimental conditions, this optimum fluence value was found to be about 30–32 J cm^{-2} (or ca. 5 GW cm^{-2} irradiance), which compares favourably with the optimum value found in the literature (3.5–4 GW cm^{-2}) for metallic samples [18]. The increase of SE with the fluence is due to the increase of the electrical field strength, and in our opinion, what works against this effect is that a higher fluence also evaporates the NPs more quickly, thereby decreasing their contribution to signal enhancement.

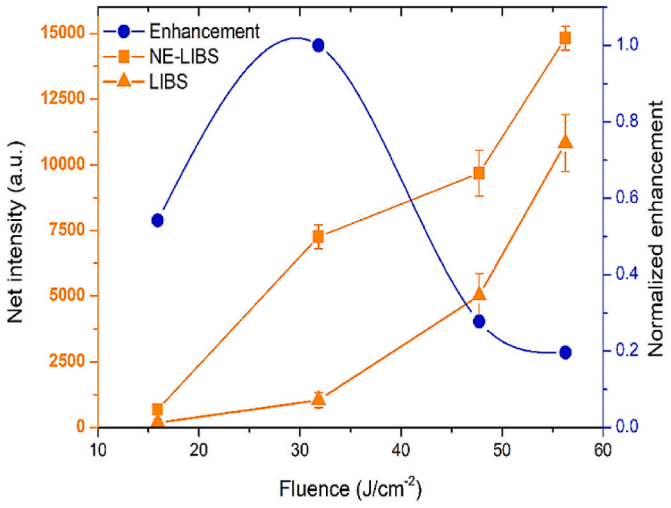

Fig. 3. The effect of laser fluence on the NE-LIBS signal enhancement on a glass sample for the Si I 288.15 nm line, using 266 nm laser pulses (all other conditions, e.g. 200 μm spot size, integrative detection, are the same as in other experiments reported in this section). Error bars represent the standard deviation based on three repetitions. The connection of data points is only meant to guide the eye.

3.1.2. Effect of detector gating

Detector gating is generally known to have a fundamental effect on LIBS signals, which are strongly transient by nature, following the evolution of the temperature and electron concentration in the plasma. However, in NE-LIBS, similar to some other signal enhancement approaches (e.g. spatial confinement), the fine optimization of the detection gate delay and gate width (integration time) has an especially high importance. It is due to that the NPs have a very short lifetime during the laser ablation process, therefore the highest SE can always be recorded with very short gate delays and gate widths. This we demonstrate in Fig. 4a., which shows that SE is highest for all spectral lines at gate delays no more than 1 μs, if a comparably short, e.g. 1 μs gate width is used. Neutral lines have somewhat longer optimal gate delays than ionic lines. These findings for the glass sample confirm similar former findings reported in the literature for metallic samples [31].

It is also worth pointing out that if emission detection is performed using longer gate widths, then the maximum SE achievable will be significantly lower. As an example, please refer to Fig. 4b., which was generated by numerically integrating the signal time profile shown in the left panel for the total lifetime of the plasma. As it can be seen, as opposed to the case with fast gating, where the maximum SE is 20–27 (depending on the spectral line), long gate width (integrated) detection only gives values between 6 and 9. Since the majority of LIBS systems used in analytical laboratories have CCD spectrometers with long, ms-range integration times, this observation partly explains why most studies attempting to reproduce the sometimes as large as two orders of magnitude NE-LIBS signal enhancements reported for sophisticated systems typically fail and can only reach single digit SE values (e.g. Refs. [20,28]). However, it is also worth considering that signal repeatability is usually better with longer integration times, thus with larger signals. It is also noteworthy that SE is largely different for insulating and conducting samples, therefore SEs for different samples can not be directly compared.

3.1.3. Effect of laser wavelength

In LIBS practice, with pulse durations in the ns regime, the sample's light absorption at the laser wavelength is very important, as it influences electron photoemission, the process that is mainly responsible for plasma ignition. In NE-LIBS, the laser pulse initiates collective electron oscillation (LSPs) in the metallic NPs and this is primarily driven by the electrical field strength, that is by laser intensity. The resonance of the laser wavelength with that of LSPs is beneficial in NE-LIBS, but it is not essential for a significant SE [18]. In addition to this, tunable laser sources are still not common in LIBS, thus fine tuning the laser wavelength to LSP resonance is more theoretical than a practical option.

Nevertheless, frequency-multipled discrete, Nd:YAG-based laser wavelengths such as 193, 213, 266, 532 nm as well as the fundamental 1064 nm are widely available in LIBS systems, thus it is worth comparing the relative effect of the wavelength on the NE-LIBS signal enhancement. We therefore performed comparative LIBS and NE-LIBS measurements using the same conditions except the laser wavelength. We tested three wavelengths, namely 266 nm, 532 nm and 1064 nm, available in our laboratory. The found SE values are shown in **Fig. 5**. As it can be seen, a monotonous decrease of the SE was observed as a function of wavelength. This trend is in accordance with the findings of

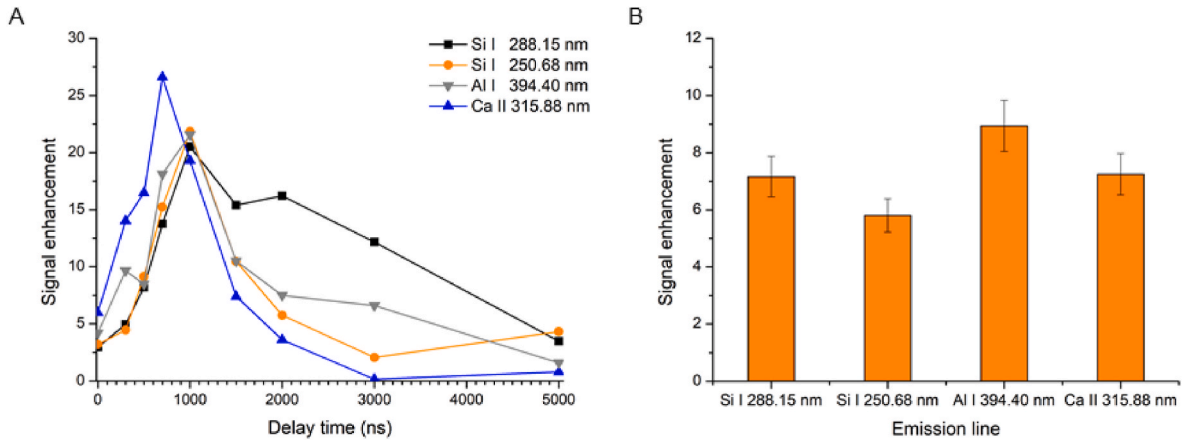

Fig. 4. Dependence of the NE-LIBS signal enhancement on detection gating as observed for a few elements (and their spectral lines) in a glass sample. A) Fast gating was used (1 μs gate width and a varied, μs-range gate delay). B) Shows the time-integrated signal enhancement, as seen by "regular" LIBS instruments with CCD spectrometers (ms-range gate width). Laser pulse energy 15 mJ and laser spot size 200 μm. All data points represent the average based on three repetitions. Error bars indicate the standard deviation.

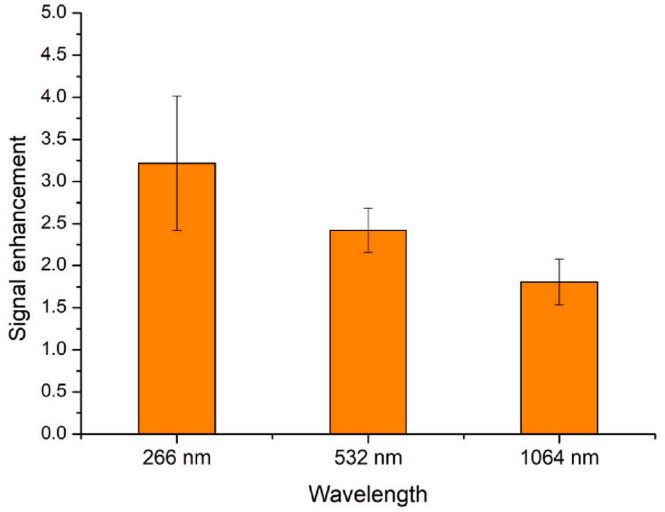

Fig. 5. Dependence of the NE-LIBS signal enhancement measured at the Si I 288.15 nm spectral line on the laser wavelength in a glass sample. Integrative detection was employed. The laser fluence was 31.77 J cm^{-2} in all cases. All conditions are the same as in other experiments reported in this section. All data points represent the average based on three repetitions. Error bars indicate the standard deviation.

Sherbini et al. [32] and Dell'Aglio et al. [17]. Now please remember that the light absorption of soda-lime glass is practically the same very low value at 532 nm and 1064 nm, whereas it is much higher in the UV. Consequently, breakdown thresholds are lower and LIBS signals are larger at 266 nm than at the other two wavelengths. At the same time, the gold spherical NPs with a diameter of 51 nm have a broad (FWHM is ca. 80 nm) light absorption, peaking at around 550 nm [33]. If the resonance of the laser wavelength with the LSP would mainly be responsible for the signal enhancement, we should see the highest SE for 532 nm. The fact, that the trend is monotonously decreasing and approximately follows the λ^{-1} dependence of the Keldysh parameter [34] indicates that in the used laser fluence regime, there is no shift in the ionization mechanism (the transition from $\gamma > 1$ to $\gamma < 1$ does not occur).

Fig. 5 suggests that under the conditions used here, a laser wavelength of 266 nm is slightly (25–50 %) better for NE-LIBS signal enhancement than the other two wavelengths. However it is notable that, due to the significant losses occurring during the harmonic laser frequency upconversion, the achievable maximum fluence from the same laser source is higher at the fundamental 1064 nm than at 266 nm. This means that one has more room for NE-LIBS signal optimalization at 1064 nm, or even at 532 nm, than at 266 nm. Therefore, from the point of view of practice, the use of all three wavelengths provide fairly comparable analytical benefits (the difference is not significant).

3.2. *Analytical applications of NE-LIBS mapping*

Our former experiments [29] described above established that using the magnetron sputtering technique for gold thin layer deposition followed by thermal treatment ("annealing") is an analytically viable sample preparation approach for acquiring NE-LIBS elemental maps. There are only two limitations in the proposed method, namely that *i)* the laser spot size, hence the spatial resolution, is only 200 μm, and *ii)* it can only be applied to samples that can withstand the 550 °C temperature of the thermal treatment. In the following sections we demonstrate the beneficial applicability of the method to geological and industrial samples. These analytical applications are mainly qualitative, but quantitative elemental mapping should also be possible, by analogy of LIBS mapping studies employing matrix-corrected signal calibration (e.g. Refs. [5,10]). In these experiments, we did not make any spectral line selection, but utilized the whole NE-LIBS hyperspectral dataset.

3.2.1. *Elemental mapping of a granite rock*

Elemental mapping of rocks by LIBS is recently gaining a lot of attention in the literature, especially when it is used for the study of the distribution of light elements, such as Li or Be, which are very important for a number of industrial sectors [35]. Prospection for various elements in mineral grains can be conveniently and efficiently done by LIBS [11,36,37].

A monzogranite type granitoid rock was used as a test sample. The rock was cut, ground and polished, followed by the complete sputtering deposition procedure described before. A 20 × 20 mm surface section was then subjected to LIBS and subsequently NE-LIBS mapping. To allow for the direct comparison of LIBS and NE-LIBS maps as much as possible, the LIBS mapping was done first, and then the surface was gently ground and polished again to remove craters and ablation debris. During this process, the condition of the surface was monitored by an optical microscope to ensure that any changes to the grain structure are as minimal as possible (only a ca. 15–20 μm thick layer of the material was removed). Then, the NP deposition (sputtering plus thermal treatment) was performed and the NE-LIBS mapping data was also collected. Step-scanning with non-overlapping laser spots was employed and the plasma

emission in the 190–1040 nm range was recorded with 0.5 μs gate delay and 1 ms gate width in each 200 μm spot, using a pulse energy of 10 mJ. The orientation and positioning of the sample between the two mapping procedures were helped to be maintained by employing deep laser-markings in the four outside corners of the sampled area. The ablation chamber was rinsed with an argon gas flow throughout the experiment. Spectral intensity-based elemental maps were then plotted by selecting and integrating a single emission line for each element of interest, and displaying their relative abundance in a colored hyperspectral image. The results can be seen in **Fig. 6** for the Li I 670.78 nm and Mg I 518.36 nm spectral lines, as examples. The signal enhancement obtained with the "slow" (ms) gating applied at the CCD spectrometer and for this non-conducting sample was about a factor of three for Li and a factor of two for Mg.

As usual, the biotite grains (which show up as black spots in the microscope image), contain a significantly higher amount of Li and Mg than the surrounding other grains (feldspar, quartz, and amphibole) [11, 37]. By comparing the microscope image of the rock taken before LIBS mapping with the elemental maps, one can appreciate that the biotite grain structure is quite well maintained, which indicates the homogeneity of the NP sample preparation procedure. The signal enhancement is clearly apparent from that finer details also show up on the NE-LIBS maps – for example, the small grains in the upper right corner of the map are only visible in the nanoparticle-enhanced case. This signal enhancement potentially also allows for a more sensitive quantitative analysis of the Li and Mg (or any other elements) in the grains. As we illustrate it in the next section, this NP-based enhancement also can be utilized for the more accurate classification of zones on a sample surface – in the case of a rock sample, these zones would be the grains.

3.2.2. *Spatial classification of black paints*

In our opinion, one of the analytical applications where NE-LIBS mapping could really shine is the spatial classification (or identification) of zones (different material qualities) within a sample, which can be achieved by applying multivariate statistical methods to the hyperspectral data set obtained. The capability of LIBS in this application area has been already demonstrated a couple of times in the literature [10, 38–40], but according to our concept, adding the signal enhancement (signal-to-noise ratio improvement) provided by gold NPs, the accuracy of the classification could be improved.

We tested this novel concept by attempting to classify five, differently branded, commercial, black thermo-paints designed for automotive use (to be used on parts exposed to extreme heat), using both the classical LIBS and also the NE-LIBS approach. The spray-paints (labeled as A to E for the purposes of this study) were delivered onto stainless steel substrates. It was also checked that the paint layers were thick enough so that the laser ablation during LIBS measurement could not penetrate them (the collected LIBS spectra were characteristic of the paint and had no contribution from the steel substrate). The black paints were similar in appearance to the naked eye; only very small shade differences could be observed. LIBS-based classification of painted steel surfaces can be useful not only in the automotive or machine industry, but in forensic science as well. Two different sample sets were prepared, one for LIBS and one for NE-LIBS analysis. On each sample, we collected 50 spectra on different locations. All other experimental conditions were as described earlier for the other samples.

The classification accuracy improvement provided by the nanoparticle-enhanced spectra was assessed by using the PCA and LDA methodologies. During our calculations data sets were randomly split in

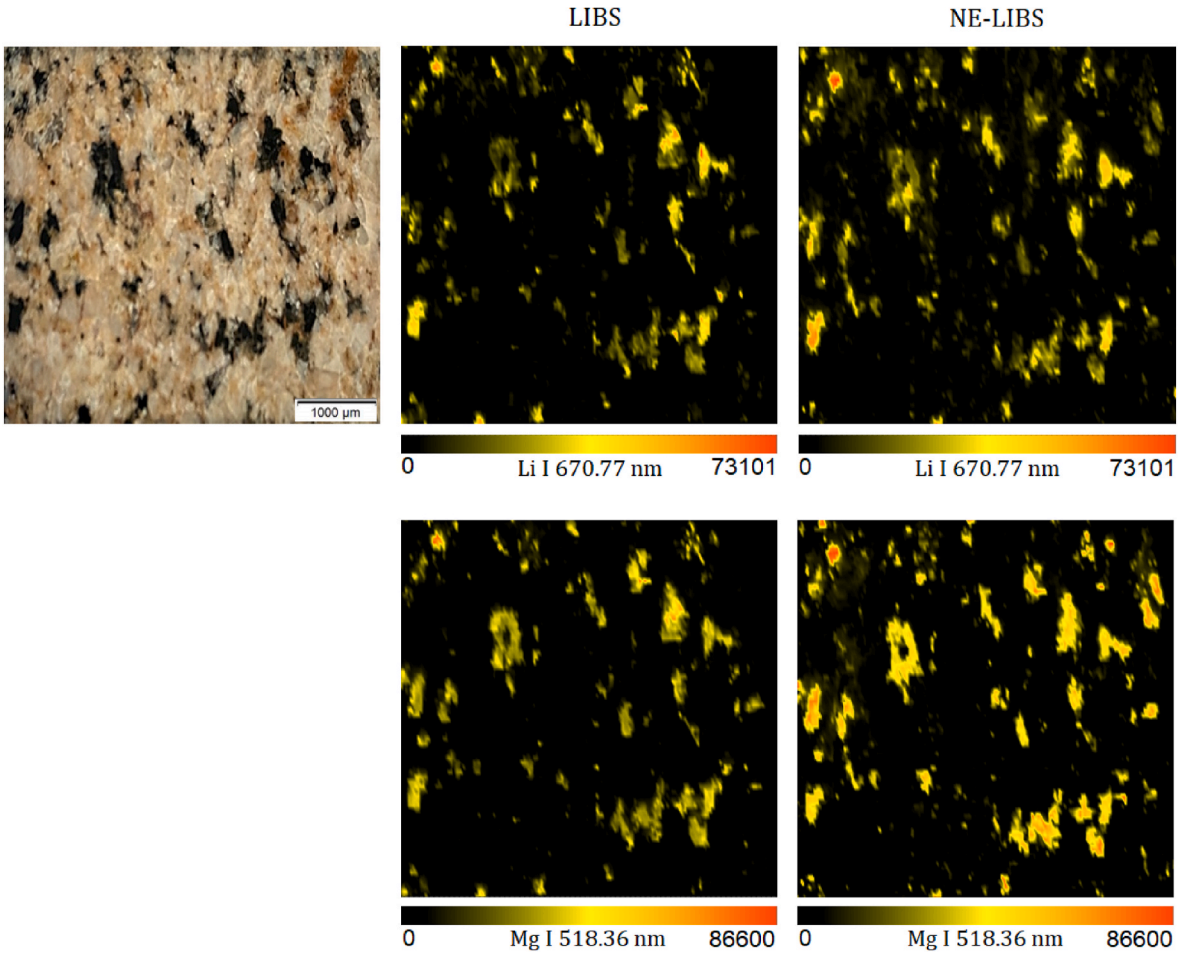

Fig. 6. Microscope image (left), as well as Li (top row) and Mg (bottom row) LIBS elemental maps recorded with and without nanoparticles.

7:3 ratio into training and validations sets. As it can be seen in Fig. 7., the separation of the data points (spectra) in the parameter space of the first three principal components is significantly better in the NE-LIBS case than in the LIBS case. Clusters of data points for paints A, B and D are strongly overlapping in the LIBS case, whereas all five clusters separate very well when nanoparticle-enhanced spectra are evaluated. The visualization of the LDA results show a similar image, but LDA also provides a numerical assessment of the accuracy of classification via the evaluation of the confusion matrices. According to our calculations, the NE-LIBS-based accuracy for the validation sets was 98.0 ± 1 %, a clear improvement over the LIBS-based accuracy of only 84.0 ± 2 % (average and standard deviation values were obtained from repeating the above calculations ten times). Please note that as the neat preparation of a patterned sample using the spray-paints was not feasible, therefore the above experiment is only meant as a demonstration of the advantageous capabilities of NE-LIBS in the spatial classification field. As a further illustration of the accuracy improvement achievable by NE-LIBS mapping, please also see Fig. 8 which is a virtual image (pattern) that contains confused pixels in the same proportions as found in the LDA confusion matrices.

4. Conclusions

We demonstrated that gold sputter-coating of the surface of solid samples followed by a thermal annealing process at 550 °C is an efficient NE-LIBS sample preparation approach for elemental mapping purposes. We also optimized the laser fluence, laser wavelength as well as detector gating from the point of view of the signal enhancement.

The usefulness of NE-LIBS hyperspectral mapping was successfully demonstrated in two qualitative analytical applications involving sample types of practical importance. The proposed NE-LIBS mapping sample preparation methodology can only be employed on solid samples which can withstand the elevated temperature needed for the thermal treatment, however such samples are not uncommon in the industry or forensic science. Some additional chemical mapping analytical tasks that can benefit from the sensitivity increase provided by NE-LIBS include, for example the investigation of glass samples in forensic research (patterns of trace contaminations can serve as evidence), quality control of colored coatings on ceramics, quality control of metal interfaces on alloys, or provenance studies of artifacts (archeology, counterfeit detection, etc.) and so. We strongly believe that the signal-to-noise improvements provided by NE-LIBS mapping are better suited for qualitative analytical discrimination applications (e.g. spatial classification or identification of the local quality of a solid sample surface) than for quantitative analysis, however the latter should also be feasible if matrix-corrected calibration is applied.

CRediT authorship contribution statement

Fernando A. Casian-Plaza: Writing – original draft, Methodology, Investigation, Data curation. **Dávid J. Palásti:** Investigation, Data curation. **Félix Schubert:** Resources, Investigation. **Gábor Galbács:**

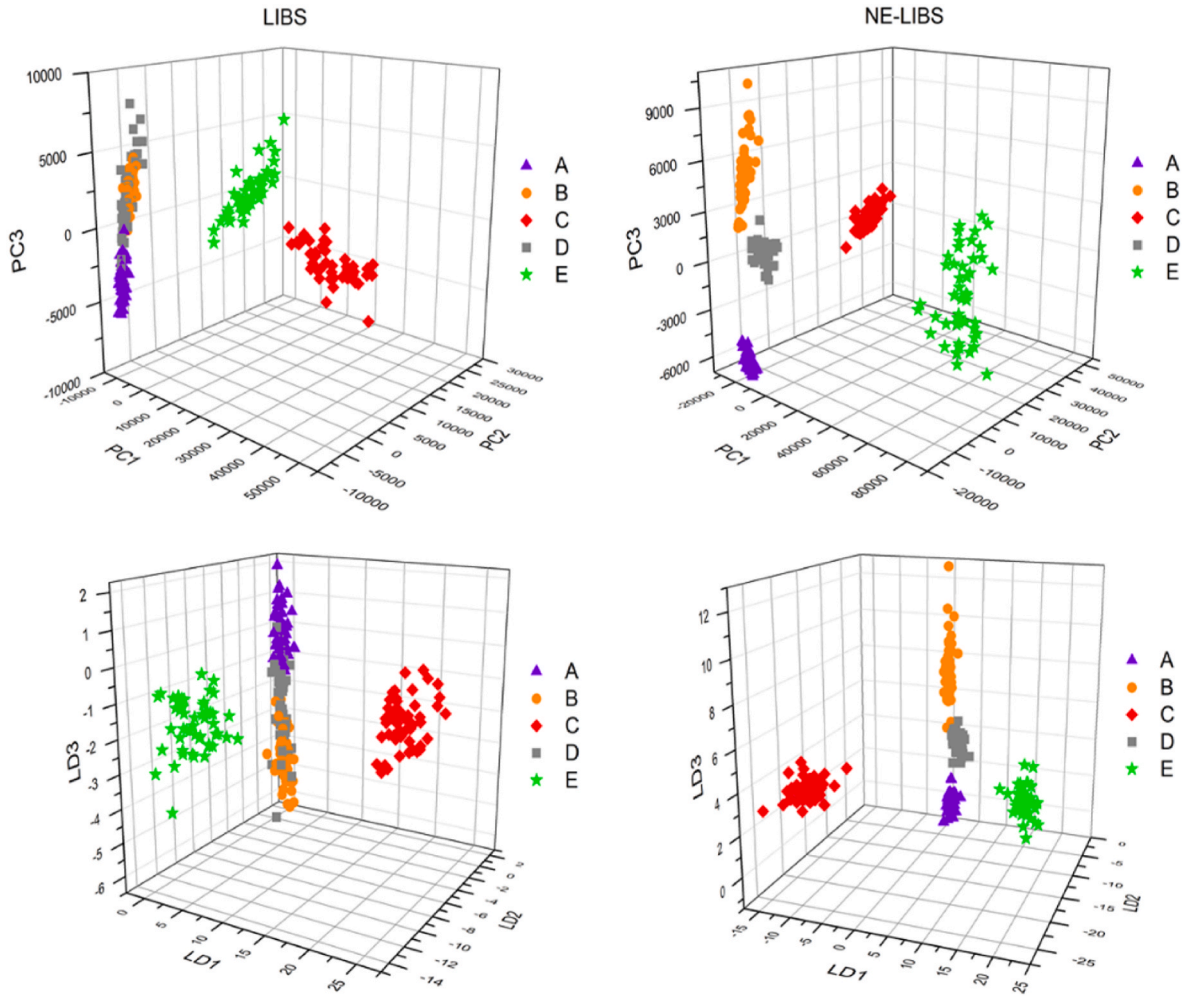

Fig. 7. Comparison of the classification of five different black paints achievable by evaluating the LIBS and NE-LIBS hyperspectral data sets using PCA (top row) and LDA (bottom row) multivariate statistical evaluation.

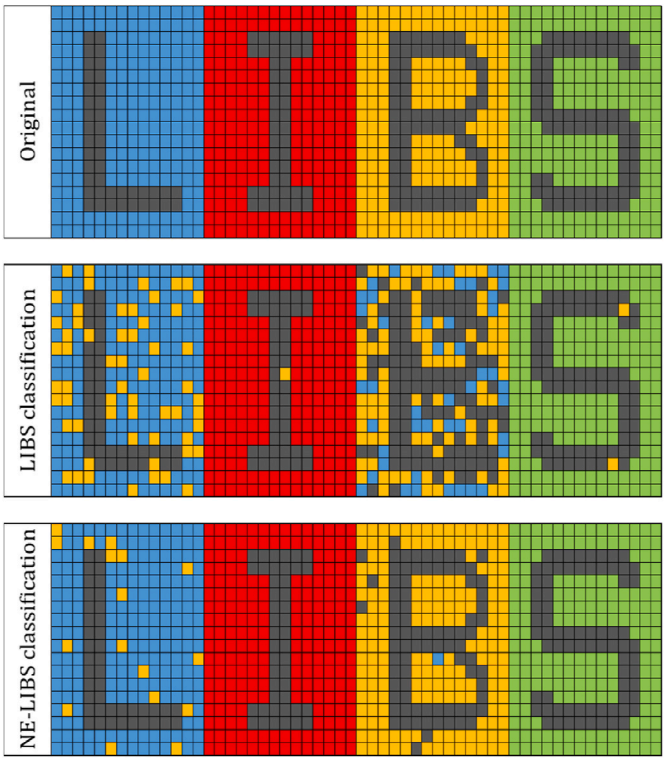

Fig. 8. A virtual image (pattern) assembled from the five paints, which contains confused pixels in the same proportions as found in the LDA confusion matrices.

Writing – review & editing, Validation, Supervision, Funding acquisition, Conceptualization.

Declaration of competing interest

The authors declare that they have no known competing financial interests or personal relationships that could have appeared to influence the work reported in this paper.

Data availability

Data will be made available on request.

Acknowledgements

The authors gratefully acknowledge the financial support from the National Research, Development and Innovation Office (NKFIH) of Hungary through TKP2021-NVA-19, K 146733. Fernando Casian-Plaza also kindly acknowledges financial support from the Consejo Nacional de Humanidades, Ciencias y Tecnologías (CONAHCYT) of Mexico through project No. 809802.

References

[1] G. Galbács, A critical review of recent progress in analytical laser-induced breakdown spectroscopy, Anal. Bioanal. Chem. 407 (2015) 7537–7562, https://doi.org/10.1007/s00216-015-8855-3.
[2] D.W. Hahn, N. Omenetto, Laser-induced breakdown spectroscopy (LIBS), Part II: review of instrumental and methodological approaches to material analysis and applications to different fields, Appl. Spectrosc. 66 (4) (2012) 347–419, https://doi.org/10.1366/11-06574.
[3] D.F. Andrade, E.R. Pereira-Filho, D. Amarasiriwardena, Current trends in laser-induced breakdown spectroscopy: a tutorial review, Appl. Spectrosc. Rev. 56 (2021) 98–114, https://doi.org/10.1080/05704928.2020.1739063.
[4] A.A. Bol'shakov, X. Mao, J.J. González, R.E. Russo, Laser ablation molecular isotopic spectrometry (LAMIS): current state of the art, J. Anal. At. Spectrom. 31 (2016) 119–134, https://doi.org/10.1039/C5JA00310E.
[5] A. Limbeck, L. Brunnbauer, H. Lohninger, P. Pořízka, P. Modlitbová, J. Kaiser, P. Janovszky, A. Kéri, G. Galbács, Methodology and applications of elemental mapping by laser induced breakdown spectroscopy, Anal. Chim. Acta 1147 (2021) 72–98, https://doi.org/10.1016/j.aca.2020.12.054.
[6] G. Galbács, Laser-induced breakdown spectroscopy, in: Biological, Forensic and Materials Sciences, first ed., Springer Nature, Switzerland, 2022.
[7] L. Jolivet, M. Leprince, S. Moncayo, L. Sorbier, C.-P. Lienemann, V. Motto-Ros, Review of the recent advances and applications of LIBS-based imaging, Spectrochim. Acta B 151 (2019) 41–53, https://doi.org/10.1016/j.sab.2018.11.008.
[8] V. Piñon, M.P. Mateo, G. Nicolas, Laser-induced breakdown spectroscopy for chemical mapping of materials, Appl. Spectrosc. Rev. 48 (2013) 357–383, https://doi.org/10.1080/05704928.2012.717569.
[9] V.K. Singh, N. Sharma, O.N. Verma, V.K. Singh, D.K. Tripathi, Y. Lee, S. Kumar, P. K. Rai, M.A. Gondal, Review: application of LIBS to elemental analysis and mapping of plant samples, At. Spectrosc. 42 (2021) 99–113, https://doi.org/10.46770/AS.2020.20.
[10] P. Janovszky, A. Kéri, D.J. Palási, L. Brunnbauer, F. Domoki, A. Limbeck, G. Galbács, Quantitative elemental mapping of biological tissues by laser-induced breakdown spectroscopy using matrix recognition, Sci. Rep. 13 (2023) 10089, https://doi.org/10.1038/s41598-023-37258-y.
[11] P. Janovszky, K. Jancsek, D.J. Palási, J. Kopniczky, B. Hopp, T.M. Tóth, G. Galbács, Classification of minerals and the assessment of lithium and beryllium content in granitoid rocks by laser-induced breakdown spectroscopy, J. Anal. At. Spectrom. 36 (2021) 813–823, https://doi.org/10.1039/D1JA00032B.
[12] M. Weiss, Z. Gajarska, H. Lohninger, M. Marchetti-Deschmann, G. Ramer, B. Lendl, A. Limbeck, Elemental mapping of fluorine by means of molecular laser induced breakdown spectroscopy, Anal. Chim. Acta 1195 (2022) 339422, https://doi.org/10.1016/j.aca.2021.339422.
[13] Y. Li, D. Tian, Y. Ding, G. Yang, K. Liu, C. Wang, X. Han, A review of laser-induced breakdown spectroscopy signal enhancement, Appl. Spectrosc. Rev. 53 (2018) 1–35, https://doi.org/10.1080/05704928.2017.1352509.
[14] G. Galbács, D.J. Palási, P.M. Janovszky, State-of-the-art analytical performance, in: G. Galbács (Ed.), Laser-induced Breakdown Spectroscopy, in Biological, Forensic and Materials Sciences, Springer Nature, Switzerland, 2022, pp. 101–127.
[15] T. Ohta, M. Ito, T. Kotani, T. Hattori, Emission enhancement of laser-induced breakdown spectroscopy by localized surface plasmon resonance for analyzing plant nutrients, Appl. Spectrosc. 63 (2009) 555–558, https://doi.org/10.1366/000370209788346896.
[16] A. De Giacomo, R. Gaudiuso, C. Koral, M. Dell'Aglio, O. De Pascale, Nanoparticle-enhanced laser-induced breakdown spectroscopy of metallic samples, Anal. Chem. 85 (21) (2013) 10180–10187, https://doi.org/10.1021/ac4016165.
[17] M. Dell'Aglio, R. Alrifai, A. De Giacomo, Nanoparticle enhanced laser induced breakdown spectroscopy (NELIBS), a first review, Spectrochim. Acta B 148 (2018) 105–112, https://doi.org/10.1016/j.sab.2018.06.008.
[18] A. De Giacomo, M. Dell'Aglio, R. Gaudiuso, C. Korala, G. Valenza, Perspective on the use of nanoparticles to improve LIBS analytical performance: nanoparticle enhanced laser induced breakdown spectroscopy (NELIBS), J. Anal. At. Spectrom. 31 (2016) 1566–1573, https://doi.org/10.1039/C6JA00189K.
[19] G. Galbács, A. Kéri, A. Kohut, M. Veres, Zs Geretovszky, Nanoparticles in analytical laser and plasma spectroscopy – a review of recent developments in methodology and applications, J. Anal. At. Spectrom. 36 (2021) 1826–1872, https://doi.org/10.1039/D1JA00149C.
[20] D.J. Palási, P. Albrycht, P. Janovszky, K. Paszkowska, Z. Geretovszky, G. Galbács, Nanoparticle enhanced laser induced breakdown spectroscopy of liquid samples by using modified surface-enhanced Raman scattering substrates, Spectrochim. Acta B 166 (2020) 105793, https://doi.org/10.1016/j.sab.2020.105793.
[21] X. Zhang, X. Li, X. Chen, M. Shi, T. Ren, Nanoparticle-enhanced laser-induced breakdown spectroscopy for serum element analysis using an Ag NP-coated filter paper substrate, J. Anal. At. Spectrom. 39 (2024) 1332–1342, https://doi.org/10.1039/d3ja00462g.
[22] D.J. Palási, L.P. Villy, A. Kohut, T. Ajtai, Z. Geretovszky, G. Galbács, Laser-induced breakdown spectroscopy signal enhancement effect for argon caused by the presence of gold nanoparticles, Spectrochim. Acta B 193 (2022) 106435, https://doi.org/10.1016/j.sab.2022.106435.
[23] Y. Cai, X. Ma, D. Ju, X. Wang, Quantitative analysis of cement raw materials based on nanoparticle-enhanced laser-induced breakdown spectroscopy, Anal. Methods 16 (2024) 4599, https://doi.org/10.1039/d4ay00644e.
[24] M. Dell'Aglio, Z. Salajková, A. Mallardi, R. Mezzenga, L. van't Hag, N. Cioffi, G. Palazzo, A. De Giacomo, Application of gold nanoparticles embedded in the amyloids fibrils as enhancers in the laser induced breakdown spectroscopy for the metal quantification in microdroplets, Spectrochim. Acta B 155 (2019) 115–122, https://doi.org/10.1016/j.sab.2019.04.002.
[25] M. Dell'Aglio, Z. Salajková, A. Mallardi, M.C. Sportelli, J. Kaiser, N. Cioffi, A. De Giacomo, Sensing nanoparticle-protein corona using nanoparticle enhanced Laser Induced Breakdown Spectroscopy signal enhancement, Talanta 235 (2021) 122741, https://doi.org/10.1016/j.talanta.2021.122741.
[26] M.R. Khan, S.U. Haq, Q. Abbas, A. Nadeem, Improvement in signal sensitivity and repeatability using copper nanoparticle-enhanced laser-induced breakdown spectroscopy, Spectrochim. Acta B 195 (2022) 106507, https://doi.org/10.1016/j.sab.2022.106507.
[27] A.A. Khedr, M.A. Sliem, M. Abdel-Harith, Gold nanoparticle-enhanced laser-induced breakdown spectroscopy and three-dimensional contour imaging of an aluminum alloy, Appl. Spectrosc. 75 (2021) 565–573, https://doi.org/10.1177/0003702820973040.

[28] Z. Xiande, C. Zhao, D. Xiaofan, D. Daming, Detecting and mapping harmful chemicals in fruit and vegetables using nanoparticle-enhanced laser-induced breakdown spectroscopy, Sci. Rep. 9 (2019) 906, https://doi.org/10.1038/s41598-018-37556-w.
[29] F.A. Casian-Plaza, P.M. Janovszky, D.J. Palásti, A. Kohut, Z. Geretovszky, J. Kopniczky, F. Schubert, S. Živković, Z. Galbács, G. Galbács, Comparison of three nanoparticle deposition techniques potentially applicable to elemental mapping by nanoparticle-enhanced laser-induced breakdown spectroscopy, Appl. Surf. Sci. 657 (2024) 159844, https://doi.org/10.1016/j.apsusc.2024.159844.
[30] K. Varmuza, P. Filzmoser, Introduction to Multivariate Statistical Analysis in Chemometrics, first ed., Taylor & Francis Group, 2009.
[31] A. De Giacomo, R. Gaudiuso, C. Koral, M. Dell'Aglio, O. De Pascale, Nanoparticle enhanced laser induced breakdown spectroscopy: effect of nanoparticles deposited on sample surface on laser ablation and plasma emission, Spectrochim. Acta B 98 (2014) 19–27, https://doi.org/10.1016/j.sab.2014.05.010.
[32] A.M. El Sherbini, C.G. Parigger, Nano-material size dependent laser-plasma thresholds, Spectrochim. Acta B 124 (2016) 79–81, https://doi.org/10.1016/j.sab.2016.08.015.
[33] P.K. Jain, K.S. Lee, I.H. El-Sayed, M.A. El-Sayed, Calculated absorption and scattering properties of gold nanoparticles of different size, shape, and composition: applications in biological imaging and biomedicine, J. Phys. Chem. B 110 (2006) 7238–7248, https://doi.org/10.1021/jp057170o.
[34] L. Keldysh, Ionization in the field of a strong electromagnetic wave, J. Exp. Theor. Phys. 20 (5) (1964) 1307–1314.
[35] European Commission, Raw materials scoreboard: European innovation partnership on raw materials. https://data.europa.eu/doi/10.2873/567799, 2021. (Accessed 27 December 2023).
[36] R.S. Harmon, C.J. Lawley, J. Watts, C.L. Harraden, A.M. Somers, R.R. Hark, Laser-induced breakdown spectroscopy—an emerging analytical tool for mineral exploration, Minerals 9 (12) (2019) 718, https://doi.org/10.3390/min9120718.
[37] K. Jancsek, P. Janovszky, G. Galbács, T.M. Tóth, Granite alteration as the origin of high lithium content of groundwater in southeast Hungary, Appl. Geochem. 149 (2023) 105570, https://doi.org/10.1016/j.apgeochem.2023.105570.
[38] L. Brunnbauer, S. Larisegger, H. Lohninger, M. Nelhiebel, A. Limbeck, Spatially resolved polymer classification using laser induced breakdown spectroscopy (LIBS) and multivariate statistics, Talanta 209 (2020) 120572, https://doi.org/10.1016/j.talanta.2019.120572.
[39] L. Pagnin, L. Brunnbauer, R. Wiesinger, A. Limbeck, M. Schreiner, Multivariate analysis and laser-induced breakdown spectroscopy (LIBS): a new approach for the spatially resolved classification of modern art materials, Anal. Bioanal. Chem. 412 (2020) 3187–3198, https://doi.org/10.1007/s00216-020-02574-z.
[40] R.H. El-Saeid, Z. Abdel-Salam, S. Pagnotta, V. Palleschi, M.A. Harith, Classification of sedimentary and igneous rocks by laser induced breakdown spectroscopy and nanoparticle-enhanced laser induced breakdown spectroscopy combined with principal component analysis and graph theory, Spectrochim. Acta B 158 (2019) 105622, https://doi.org/10.1016/j.sab.2019.05.011.